

Extending the Law of Intersegmental Coordination: Implications for Powered Prosthetic Controls

Elad Siman Tov¹ and Nili E. Krausz²

Abstract—Powered prostheses are capable of providing net positive work to amputees and have advanced in the past two decades. However, reducing amputee metabolic cost of walking remains an open problem. The Law of Intersegmental Coordination (ISC) has been observed across gaits and has been previously implicated in energy expenditure of walking, yet it has rarely been analyzed or applied within the context of lower-limb amputee gait. This law states that the elevation angles of the thigh, shank and foot over the gait cycle are not independent. In this work, we developed a method to analyze intersegmental coordination for lower-limb 3D kinematic data, to simplify ISC analysis. Moreover, inspired by motor control, biomechanics and robotics literature, we used our method to broaden ISC toward a new law of coordination of moments. We find these Elevation Space Moments (ESM), and present results showing a moment-based coordination for able bodied gait. We also analyzed ISC for amputee gait walking with powered and passive prosthesis, and found that while elevation angles remained planar, the ESM showed less coordination. We use ISC as a constraint to predict the shank angles/moment that would compensate for alterations due to a passive foot so as to mimic a healthy thigh angle/moment profile. This may have implications for improving powered prosthetic control. We developed the ISC3d toolbox that is freely available online, which may be used to compute kinematic and kinetic ISC in 3D. This provides a means to further study the role of coordination in gait and may help address fundamental questions of the neural control of human movement.

I. INTRODUCTION

Transfemoral amputees have been shown to have elevated metabolic cost when walking compared to able-bodied gait [1] as well as commonly exhibiting prominent hip compensations, such as circumduction [2]. Typically these individuals are clinically prescribed a microprocessor knee (MPK) and a passive prosthetic foot (e.g. carbon-fiber dynamic response feet). These devices dissipate energy and cannot provide positive power which might explain elevated metabolic cost for amputees [3]. In the past several decades researchers have developed powered prostheses [4], [5] capable of providing net positive work to the amputee, with the goal of reducing metabolic cost [6].

Over the past two decades above-knee powered prostheses have typically used joint level impedance control at the knee and ankle [4]. Inspired by [7], for each desired gait behavior the torque-angle relationship at each joint is parameterized

over discrete phases of the gait cycle. Recently, state-of-the-art powered prosthesis controllers expand on this approach by estimating a continuous gait *phase variable* to parameterize their control law for the knee and ankle joints over the gait cycle [8]. This control method can enable a wide variety of gait behaviors; however, there remain existing limitations with this approach. For example, understanding how changes in knee or ankle parameters affect energetic cost or induce unwanted hip compensations is challenging.

An important result that may have implications for reducing metabolic cost and hip compensations in amputee gait was presented almost two decades ago [9]. Researchers showed a relationship between the mechanical energy of walking and the kinematic coordination of the human leg in elevation angles (segment orientations as measured from the global vertical axis). While it is standard to present kinematic data in joint angles, elevation angles have been observed to follow the so-called Law of Intersegmental Coordination (ISC) [10]. ISC describes a coordination phenomenon that has been observed across gaits, speeds, and inclines [9]–[14] whereby the elevation angles of the thigh, shank, and foot segments (when measured in the sagittal plane) form trajectories that covary along a plane (termed the Covariation Plane or CVP). The tilt of the CVP was found by [9] to be tied to the mechanical energy cost at a wide range of gait speeds. Although ISC is a kinematic determinant of human locomotion [10], the study of ISC in the context of amputee gait has been limited [15].

There are clear implications of ISC for powered prosthetics. Due to the phase-based parameterization, the existing controllers used by ankle-knee prostheses implicitly impose a *coupling* between joints, whether in joint angles, joint torques, or even joint level impedance. Even in a decoupled control architecture, when parameterizing both joint-level knee and ankle controllers by a single phase variable their references do not change independently. This approach originated from bipedal robot control methods (see [16]), and has been implemented in experimental powered prosthetic devices for multiple locomotion tasks [17]–[21]. In [22] an alternate control based on adaptive control method was presented that explicitly couples the joint controllers (without the use of a phase variable) with position and torque synergies between joints. Thus, current control methods of powered prostheses aim at achieving a coordinated gait, without explicitly considering ISC.

In this work, we analyze ISC in amputee gait with powered prostheses and compare to behavior of able-bodied individuals. We present a new method for transforming reported joint

*This work was funded by the Israel Science Foundation grant 2937/24

¹Elad Siman Tov is with the Faculty of Mechanical Engineering, Technion – Israel Institute of Technology, 32000 Haifa, Israel
elad.sim@campus.technion.ac.il

²Nili E. Krausz is with the Faculty of Mechanical Engineering, Technion – Israel Institute of Technology, 32000 Haifa, Israel
nili.krausz@technion.ac.il

angles into elevation angles, which can then be used to assess ISC. We hypothesize that joint moments in a transformed elevation angle space will also covary as do the kinematics, and present a novel approach for finding *elevation space moments* (ESM). Joint moments in the sagittal plane have been previously shown to be related to one another by the *Total Support Moments* (see [23], [24]). Winter claimed this support moment suggests a compensatory mechanism where joint moments compensate for one another. Inspired by this work and the ISC, we evaluate the potential coordination of ESM to assess whether dimensionality reduction exists for moments as well as kinematics in elevation angle coordinates. We also consider how this dimensionality reduction may be altered in amputee gait. Our conjecture, is that a deeper understanding of these phenomena could lead to a unified theory of dynamic coordination that may have potential as a new paradigm for control of powered prosthetic legs.

II. METHODS

A. Datasets

Two datasets were used. An open dataset of 10 Able Bodied (AB) individuals including walking, running and stair ascent/descent activities in variable inclines and speeds [25]; and a dataset of 3 Transfemoral Amputees (TFA) walking at variable speeds, with their prescribed passive prosthesis and a powered prosthesis [26]. Both datasets were recorded using Vicon motion capture system accompanied by an instrumented treadmill (Bertec). In this work, for both datasets we analyzed steady-state walking, with zero incline over three speeds. The AB individuals walked at speeds (0.8[m/s], 1.0[m/s], and 1.2[m/s]), and each of the three amputees (TFA1, TFA2, TFA3) walked at a slow (0.9[m/s], 0.8[m/s], 0.8[m/s]), normal (1.1[m/s], 1.0[m/s], and 1.0[m/s]) and a fast (1.3[m/s], 1.2[m/s], and 1.2[m/s]) self selected speed, respectively. Joint moments are given as [Nm/kg], normalized by body-weight.

B. Elevation Angle Covariation Plane

The elevation angles of the thigh (α_t), shank (α_s), and foot (α_f) are computed using the transformation as will be described in section II-C. The Covariation Plane (CVP) is the visual representation of elevation angle coordination. Principal Component Analysis (PCA) was performed for all trials to evaluate intersegmental coordination as in [9]–[11]. The projections of the thigh, shank, and foot trajectories onto the PC vectors are referred to as the PC scores. The Planarity Index (PI) is defined as the variance accounted for by the first two PCs, and used to quantify the level of planarity of the CVP. Larger values imply a stronger planar dependency between variables as in [14]. Here λ_i is the i^{th} PC variance, i.e. the i^{th} eigenvalue of the covariance matrix.

$$PI = \frac{\lambda_1 + \lambda_2}{\lambda_1 + \lambda_2 + \lambda_3} \cdot 100\% \quad (1)$$

In addition to evaluating the CVP and PI, the coupling at the shank-foot is considered and the linear portion associated with the swing phase of gait was fit with a linear model.

C. Transforming Joint Angles To Elevation Angles

Elevation angles have been used to analyze intersegmental coordination. However, these studies have traditionally computed elevation angles directly from surface markers to approximate segment axes. This creates a computational challenge that skips the use of established motion capture software, and is inconsistent with standard definitions of anatomical joint angles and joint center estimates. Moreover, this leads to challenges in making broader comparisons about intersegmental coordination, as most human gait studies present data in terms of joint angles. Therefore, a general method to compute elevation angles from previously published joint angle data was needed. Our algorithm utilizes 3D anatomical angles computed by motion capture systems to estimate the elevation angles of the leg segments. This transformation between joint and elevation angles also provides an analytical method for transforming velocities and moments into an elevation coordinate frame, which will be shown in section II-D.

We denote the flexion angle as ϕ , the adduction angle as δ , and the rotation angle as ρ , with the lower script to represent the corresponding joint (i.e., knee flexion ϕ_k and hip internal rotation as ρ_h). Given the pelvis absolute angles (ϕ_p, δ_p, ρ_p) with respect to a subject global reference frame (following ISB recommendations [27]), the orientation of the pelvis segment frame (R_p) is found by the intrinsic multiplication of rotation matrices in the conventional order for the pelvis (Pelvic Tilt, Obliquity, Rotation).

$$R_p = R_z(\phi_p) R_x(\delta_p) R_y(\rho_p) \quad (2)$$

Similarly, the thigh (R_t), shank (R_s), and foot (R_f) segment frame orientations were found using the anatomical hip, knee, and ankle angles, with rotations in the conventional order (see Appendix Table II).

$$R_t = R_p R_z(\phi_h) R_x(\delta_h) R_y(\rho_h) \quad (3)$$

$$R_s = R_t R_z(\phi_k) R_x(\delta_k) R_y(\rho_k) \quad (4)$$

$$R_f = R_s R_z(\phi_a + 90^\circ) R_x(\rho_a) R_y(\delta_a) \quad (5)$$

The elevation angular velocity vector is found using the skew-symmetric matrix representation of angular velocity of each segment ($\Omega_i \in so(3)$), computed by the rotation matrices ($R_i \in SO(3)$), and their element-wise derivatives (\dot{R}_i) for a fixed frame [28].

$$\Omega_i = \dot{R}_i R_i^T \quad (6)$$

Here the components of the angular velocity vector represented by Ω_i are the i^{th} segment angular velocities in three axes (sagittal, frontal, transversal) in a subject fixed global frame. The angular velocities of each segment i are found by selecting its components from Ω_i , as shown in (7). For the left leg (Ω_i^L), the rotations ($\alpha_i, \beta_i, \gamma_i$) are about (+Z,-X,-Y) axes, and for the right leg (Ω_i^R), the ($\alpha_i, \beta_i, \gamma_i$) rotations are about (+Z,+X,+Y) axes in an ISB recommended frame [27].

$$\Omega_i^R = \begin{bmatrix} 0 & -\dot{\alpha}_i & -\dot{\gamma}_i \\ \dot{\alpha}_i & 0 & \dot{\beta}_i \\ \dot{\gamma}_i & -\dot{\beta}_i & 0 \end{bmatrix} \quad \Omega_i^L = \begin{bmatrix} 0 & -\dot{\alpha}_i & \dot{\gamma}_i \\ \dot{\alpha}_i & 0 & -\dot{\beta}_i \\ -\dot{\gamma}_i & \dot{\beta}_i & 0 \end{bmatrix} \quad (7)$$

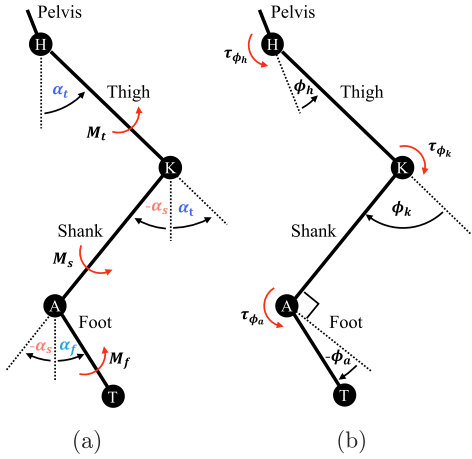


Fig. 1: Schematic of (a) elevation angles (α_i) and moments (M_i) in the sagittal plane, and (b) anatomical joint flexion angles (ϕ_j) and their internal joint torques (τ_{ϕ_j}). Ankle dorsiflexion is assumed as positive. All moments are defined in the positive direction of their associated angle.

In this work we consider only the elevation angular velocities in the sagittal plane ($\dot{\alpha}$) using (8), because we observe coordination in the α spanned vector space. In future work, we will consider 3D coordination including the β_i, γ_i angles.

$$\dot{\alpha} = [\Omega_{t,(2,1)}, \Omega_{s,(2,1)}, \Omega_{f,(2,1)}]^T \quad (8)$$

For each segment i its elevation angle α_i is computed using the projection of the segment axis onto the sagittal plane as in (9). This is consistent with formulas presented in [10].

$$\alpha_i = \text{atan}2(-R_{i,(1,2)}, R_{i,(2,2)}) \quad (9)$$

Consider a simplified 2D case in the sagittal plane shown in Fig. 1, where out-of-plane terms ($R_x(\cdot)R_y(\cdot)$) are ignored. Under these conditions, (9) reduces to a relation between joint flexion angles (ϕ_j) and sagittal plane elevation angles (α_i) given in (10) (see Appendix Table II for sign corrections).

$$\begin{bmatrix} \alpha_p \\ \alpha_t \\ \alpha_s \\ \alpha_f \end{bmatrix} = \begin{bmatrix} -\phi_p \\ -\phi_p + \phi_h \\ -\phi_p + \phi_h - \phi_k \\ -\phi_p + \phi_h - \phi_k + \phi_a + 90^\circ \end{bmatrix} \quad (10)$$

Accordingly, we obtain a transformation between joint angle and elevation angle velocities in the sagittal plane (11).

$$\begin{bmatrix} \dot{\alpha}_p \\ \dot{\alpha}_t \\ \dot{\alpha}_s \\ \dot{\alpha}_f \end{bmatrix} = \begin{bmatrix} -\dot{\phi}_p \\ -\dot{\phi}_p + \dot{\phi}_h \\ -\dot{\phi}_p + \dot{\phi}_h - \dot{\phi}_k \\ -\dot{\phi}_p + \dot{\phi}_h - \dot{\phi}_k + \dot{\phi}_a \end{bmatrix} \quad (11)$$

D. Elevation Space Moments (ESM)

In robotics, a typical method to map generalized force vectors between joint space and task space uses the Jacobian and its pseudo-inverse [29]. Inspired by this approach, we define a *reduced elevation space Jacobian* ($J_\alpha \in \mathbb{R}^{3 \times 12}$), to transform anatomical joint moments (τ) to their projected moments in the elevation angle space (M) as shown in (12)

$$M = (J_\alpha^T(q))^\dagger \tau \quad (12)$$

where $M = [M_t, M_s, M_f]^T$ is the sagittal plane elevation space moments, q is the vector of 3D anatomical angles of the pelvis, hip, knee and ankle joints, and τ is the vector of 3D moments in joint space (see Appendix A). The 3D transformation described in section II-C was used to derive $J_\alpha(q)$. Specifically, $J_\alpha(q)$ maps anatomical joint velocities (\dot{q}) to segment elevation velocities ($\dot{\alpha} = [\dot{\alpha}_t, \dot{\alpha}_s, \dot{\alpha}_f]^T$) for the thigh, shank, and foot. We focus on the thigh, shank and foot in the sagittal plane because intersegmental coordination is traditionally viewed in these terms.

$$\dot{\alpha} = J_\alpha(q)\dot{q} \quad (13)$$

Note that J_α is a reduced Jacobian because it projects 12-DOF joint space into a 3-DOF sagittal elevation space. The evaluation of this assumption is further discussed in section II-E. We derived $J_\alpha(q)$ from (8) using the MATLAB Symbolic Math Toolbox. The algorithm was implemented in our ISC3d toolbox which can be freely accessed online [30].

Similar to coordination in elevation angle space, we expect to find coordination in the elevation space moments. To quantify this coordination, we use the Planarity Index as described in (1) (see section II-B).

E. Interpretation of Elevation Space Moments

Based on the simplified 2D case in (10) and (11), we can better understand the ESM. Because the total instantaneous external power generated (P_T) is invariant to the coordinates in which it is represented, P_T can be given as the sum of products of internal joint torques and the relative joint velocities (defined in the same directions). Thus, a simplified version of elevation space moments, are given as the combined joint torques terms (τ_{ϕ_j}) on the right hand side of (14).

$$P_T = \begin{bmatrix} 0 \\ \tau_{\phi_h} \\ \tau_{\phi_k} \\ \tau_{\phi_a} \end{bmatrix}^T \begin{bmatrix} \dot{\phi}_p \\ \dot{\phi}_h \\ \dot{\phi}_s \\ \dot{\phi}_f \end{bmatrix} = \begin{bmatrix} -\tau_{\phi_h} \\ \tau_{\phi_h} + \tau_{\phi_k} \\ -\tau_{\phi_k} - \tau_{\phi_a} \\ \tau_{\phi_a} \end{bmatrix}^T \begin{bmatrix} \dot{\alpha}_p \\ \dot{\alpha}_t \\ \dot{\alpha}_s \\ \dot{\alpha}_f \end{bmatrix} \quad (14)$$

In this work, we compute ESM using (12). Although we use 3D anatomical angles (q), we focus on a reduced elevation space in the sagittal plane (α , $\dot{\alpha}$ and M). To evaluate our reduced method (J_α), we compare the the total instantaneous power computed in the joint space ($P_T = \tau^T q$) with the total instantaneous power computed in moment space ($P_T = M^T \dot{\alpha}$).

F. The CVP as a constraint

We consider how planar coordination could be leveraged as a constraint for estimating the desired behavior of a given segment towards prosthesis control. The CVP could be used to reduce the dimensionality of the prosthesis control problem. For a given measured foot behavior we can estimate a desired shank profile that may reduce thigh compensation (i.e. achieve healthy kinematics and dynamics of the subject's thigh), using the estimated planar covariation of the elevation angles and the ESM. Our conjecture is that by controlling a prosthesis to coordinate appropriately, we may reduce unwanted compensatory movements. While in this work we

do not simulate the desired controller, we impose a constraint of the CVP to predict how the shank could compensate for a passive prosthetic foot while attempting to achieve healthy thigh behavior. The predicted shank profile can then be compared to the actual amputated leg behavior.

Let the elevation angle CVP be defined by the constraint $g_\alpha(\alpha_t, \alpha_s, \alpha_f) = 0$ and the elevation space moments CVP as $g_M(M_t, M_s, M_f) = 0$. The thigh components are given by a mean value of the AB subject, and the foot components are taken from the TFA (Passive) foot behavior. Thus, the predicted shank angle/moment profile for coordination, is found in (15) and (16), respectively.

$$\alpha_s = f_\alpha(\alpha_t, \alpha_f) \quad (15)$$

$$M_s = f_M(M_t, M_f) \quad (16)$$

See section III-E for example results from this approach.

III. RESULTS

A. Elevation Angle Covariation

The elevation angles over the gait cycle are shown in Fig. 2. The profiles of the mean thigh, shank, and foot elevation angles are shown across three speeds for each condition, showing asymmetries in amputee gait on both passive and powered legs. Specifically, the amputated leg has its peak elevation angle earlier in the gait cycle. The CVP results for AB and TFA subjects are given in Fig. 3, showing dimensionality reduction across all three conditions. Critically, the shape of the covariation on the plane differs for the amputated leg, with noticeable changes occurring during early stance.

The PC scores (see Fig. 4) show a planar coordination with a maximal out of plane component of 10.37° for AB, 8.86° for TFA passive, and 15.1° for TFA powered. Additionally, PC1 shows remarkable similarity to the shank and foot elevation angles implying some level of foot-shank coupling, and PC2 shows similarity to the thigh elevation angle Fig. 2. The shank-foot coupling is shown more explicitly in Fig. 5, and is quantified in Table I, where the slope and bias were assessed for the linear portion of shank-foot coupling associated with swing. The passive leg has a steeper slope and stronger negative bias of approximately 10° compared to that of the AB subjects. Meanwhile, the powered leg trended in the opposite direction, with a shallower slope and lower negative bias of over 10° relative to that of AB subjects.

TABLE I: Slope and Bias of the linear portions for all strides in the shank-foot coordination (mean plots shown in Fig. 5). All fits achieved a mean R^2 value greater than 0.9890 with a near perfect fit in the amputated leg of the passive case ($R^2 = 0.9998 \pm 0.0003$).

Case	Leg	Slope	Bias (deg)
Able Bodied	—	0.86 ± 0.05	-80.45 ± 3.78
Passive	Amp.	1.00 ± 0.01	-90.44 ± 2.37
	Con.	0.82 ± 0.05	-79.01 ± 4.75
Powered	Amp.	0.71 ± 0.05	-59.01 ± 3.91
	Con.	0.83 ± 0.07	-77.89 ± 5.13

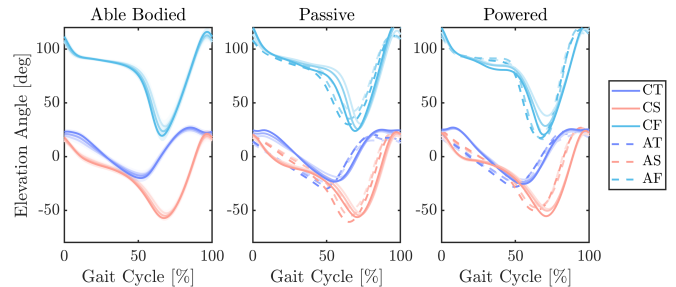


Fig. 2: Elevation angles of the thigh (T), shank (S) and foot (F) computed from (9). Able bodied mean curves with shaded standard deviations (left), amputees with a passive prosthesis (middle) and amputees with a powered prosthesis (right). The amputated (A) side is indicated by a dashed line, and the contralateral (C) side as a solid line, as in AB data. For this and Figs. 3 to 5, 7, 8 and 10 means across subjects for three speeds are shown; slower speeds correspond to more transparent colors.

B. Planarity Index (PI)

The elevation angle Planarity Index is presented in Fig. 6a. Across all conditions the mean planarity index was $> 99\%$, showing a high level of planar covariation. The ESM Planarity Index only showed high mean planarity values ($> 98\%$) for the AB and contralateral legs; however, the amputated legs showed greater variance and lower mean planarity scores of $97.8 \pm 1.3\%$ and $95.9 \pm 2.4\%$ for the passive and powered legs, respectively.

C. Elevation Space Moments (ESM)

The ESM are shown in Fig. 7 for AB and TFA subjects across speeds. The elevation moments are strikingly altered between TFA and AB conditions. Particularly, the shank and foot moments are substantially decreased for both the contralateral and amputated legs. The PCs of the ESM (see Fig. 8) show a similar coupling between the shank and foot as previously described for elevation angles. Importantly, the amputee results demonstrate altered PC scores relative to AB subjects, with large differences between amputated and contralateral legs, reflecting changes to the shank and foot moments as described in Fig. 7. However, PC2 for the contralateral leg of TFA subjects is similar to AB subjects.

D. Power Evaluation

The total mechanical power was computed for AB individuals both in joint space ($P_T = \tau^T \dot{q}$) and in elevation space ($M^T \dot{\alpha}$) variables are presented in Fig. 9. Agreement was quantified using the coefficient of determination $R^2 = 0.91 \pm 0.07$ and a range-normalized RMSE of $6.5\% \pm 2.2\%$.

E. Predicted Shank Profile

The results for our predicted shank elevation angle profile based on the CVP constraint are shown in Fig. 10a. Comparing the predicted shank elevation angle to the AB and TFA (Passive) profiles, reveals that to adhere to the CVP of AB subjects, for much of the gait cycle, the shank should be moving with a similar elevation angle to that of AB subjects. However, during terminal-stance/early swing, the shank angle magnitude should be reduced to compensate for

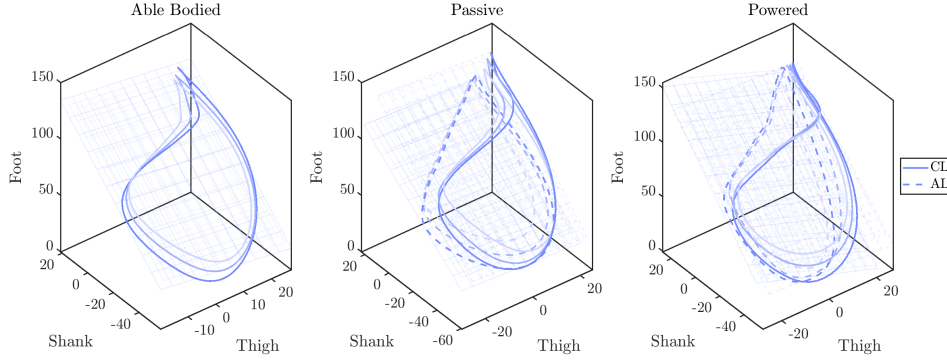


Fig. 3: Elevation angles Covariation Plane. The amputated leg (AL) is indicated by a dashed line, and contralateral leg (CL) as a solid line. The plane of each loop, defined by the first and second PCs, is shown as a grid. The trajectory progresses in gait phase counterclockwise. The top (bottom) of the loop is linked to the heel strike (toe-off) events, respectively.

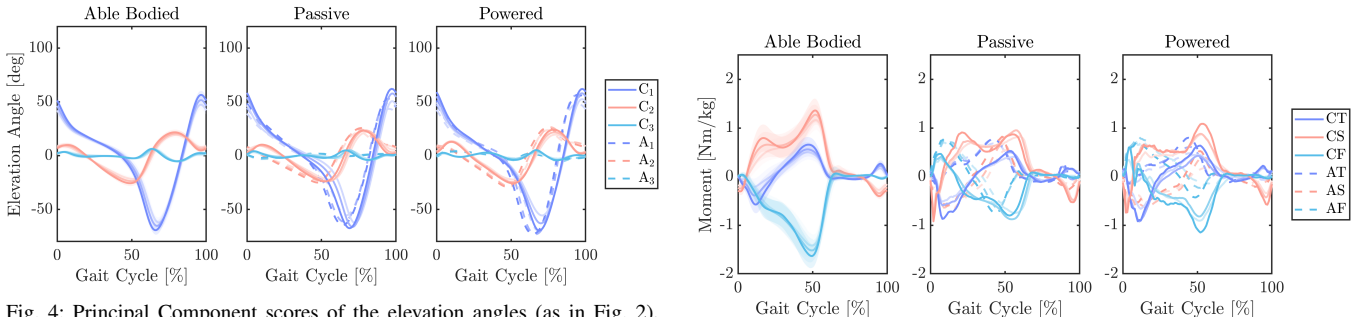


Fig. 4: Principal Component scores of the elevation angles (as in Fig. 2), with indices ordered by decreasing PC variance for amputated (A) and contralateral (C) legs.

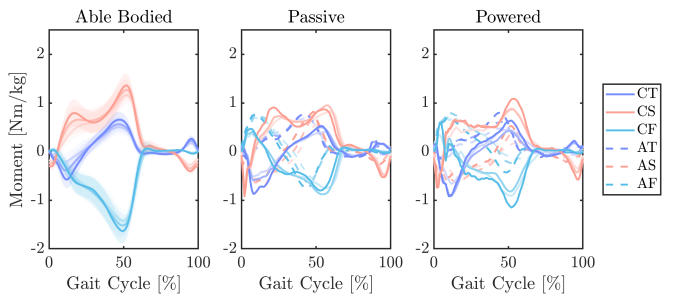


Fig. 7: Elevation space moments computed from (12).

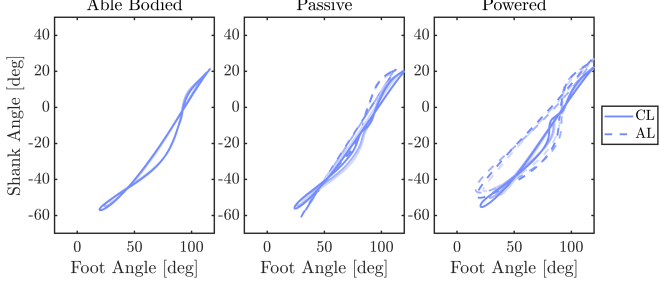


Fig. 5: Mean Shank-Foot coordination which is adopted from [10].

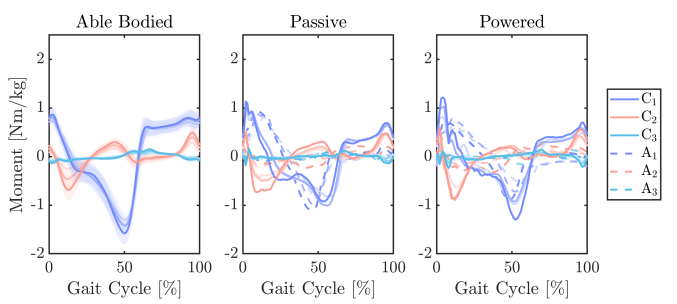


Fig. 8: Principal Component scores of the elevation space moments shown in Fig. 7.

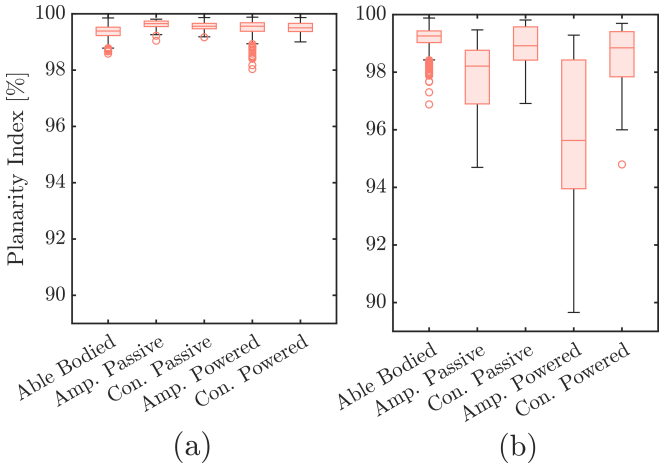


Fig. 6: Planarity Index compared between Able Bodied, Contralateral (Con.) and Amputated (Amp.) cases for (a) elevation angles and (b) elevation space moments.

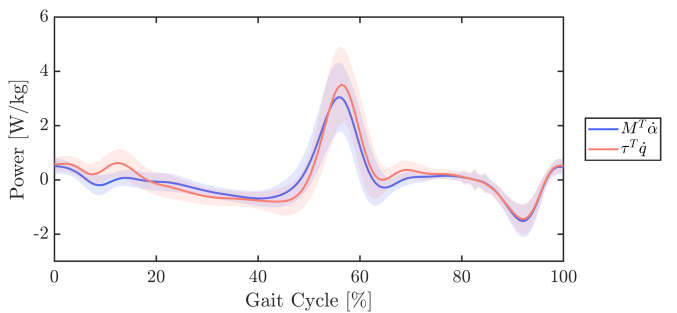


Fig. 9: Means across AB subjects of the sum of internal joint powers in all 3 anatomical axes (red) compared with the sum of powers computed using the ESM in (12), and the elevation angle velocities in (8) (blue).

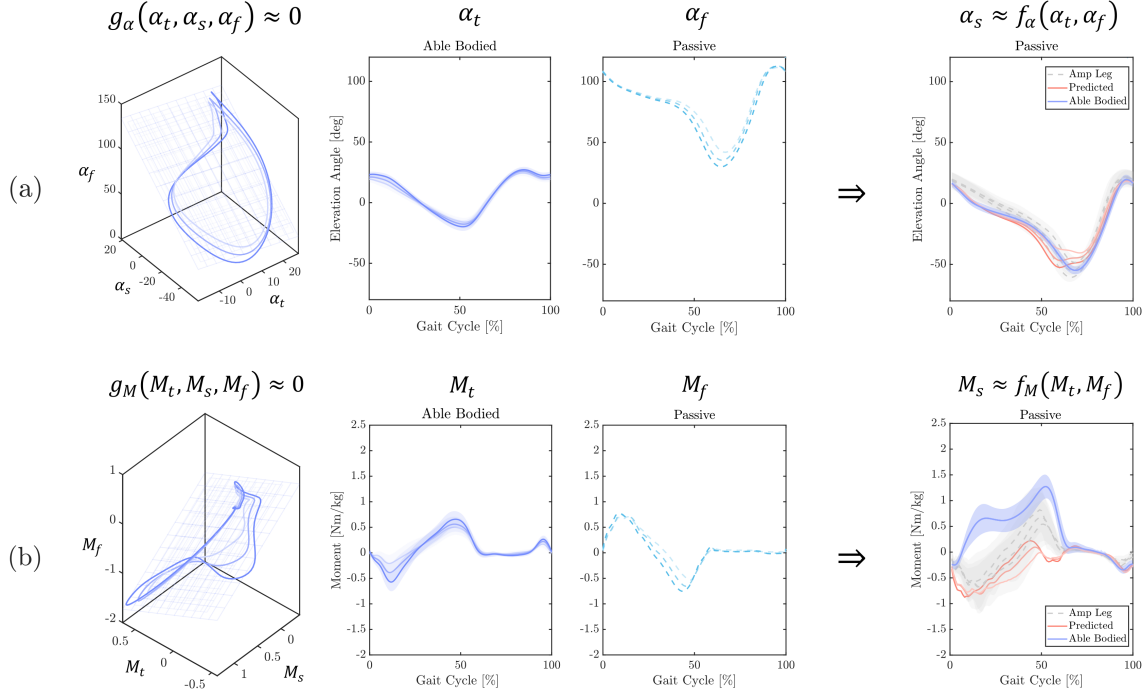


Fig. 10: Demonstration of using the CVP as a constraint shown on left for (a) elevation angles, and (b) elevation space moments to reduce the dimensionality of the coordination problem in control. For each variable (angle/moment) we attempt to mimic healthy thigh (α_t, M_t) and predict the shank behavior (α_s, M_s) that would be required to compensate for the passive prosthetic foot (α_f, M_f) and that would comply with healthy CVP. The AB shank (blue solid line) and amputated Passive shank (grey dashed line) angle/moment are shown for comparison on the right.

the altered passive foot angle. The predicted shank elevation space moments are shown in Fig. 10b. When constrained to comply with a planar law, our predicted shank moment is found to be lower than that currently achieved by the amputated leg during terminal stance with the passive prosthetic foot.

IV. DISCUSSION AND CONCLUSION

In this work we evaluate coordination of gait for AB and TFA subjects. Figures 2 to 4 show that covariation of elevation angles occurs in amputee gait, but it is altered with respect to AB subjects. To our knowledge, this is the first ISC analysis of amputees walking with powered devices. We evaluated Planarity Index for elevation angles and found high mean values of $> 99\%$ showing clear dimensionality reduction (see Fig. 6a).

The dimensionality reduction as shown by PI is to a large extent due to the coordination of the shank and foot (see Fig. 5). Comparing the shank-foot coordination of the amputated and contralateral legs we note a distinct difference: while the contralateral leg has a slope and bias close to that of the able-bodied individuals, the amputated leg has a clear offset. For the passive leg the slope of the linear portion of the shank-foot coordination for the amputated leg was 1.00 ± 0.01 as shown in Table I, implying that the shank and foot moved as rigid bodies, with no ankle flexion during the swing phase. Moreover, for the powered leg the results correspond to the decreased peak shank elevation angle and increased peak foot elevation angle during walking, as

shown in Fig. 2. Thus the addition of power in this case is insufficient for resolving the coordination of the amputated leg during swing.

In this work we presented a method and results for transforming moments from joint space to elevation space. Evaluating the elevation space moment results in Fig. 7, we find a surprisingly high level of coordination between the moments in this elevation space for AB gait. This is shown in Fig. 6b, where the mean PI of elevation space moments for AB gait was found to be $> 99\%$ and further highlighted in the PC scores as shown in Fig. 8 where the PCs show distinct dimensionality reduction with little variance accounted for by PC3 for AB subjects.

The elevation space moments in Fig. 7, showed a lack of coordination which differed greatly from that of AB subjects and differed from TFA elevation angles which were altered, yet remained coordinated. These results highlight the reduced ESM coordination of both the passive and powered legs as compared to AB subjects. This was further highlighted in the results of the ESM Planarity Index (see Fig. 6b). Particularly of note is that while the contralateral leg achieved fairly similar PI values as compared with AB subjects, the amputated leg had substantially decreased planarity, and higher standard deviations versus AB and contralateral legs (3.4x and 6.8x as high for the passive and powered legs, respectively).

The results of this work are promising; however, there are several limitations we aim to address in future work. The size of the dataset analyzed was fairly small, particularly

for TFA subjects with only three individuals walking on their prescribed passive and on a powered leg. Moreover, we only considered walking conditions on a treadmill with no incline and a small range of speeds. In the future, we aim to expand our analysis to include a larger number of subjects and conditions. Additionally, we plan to test the effect of perturbing ISC and we will also include assessments of metabolic cost of transport to further validate the relationship between ISC and energetics.

The clear alteration in coordination for amputee gait may stem from the lack of a means for assessing and controlling coordination in an explicit manner in current prosthetic systems. While the parameterization of gait phase variables implicitly imposes some coupling between degrees of freedom, an *explicit* heuristic to coordinate biomimetically has yet to be implemented to our knowledge. While this was yet to be demonstrated in a real-time approach, we suggest that such a heuristic could inform a new paradigm for prosthetic controls whereby coordination is imposed as a constraint to reduce the dimensionality of the control problem.

Such a heuristic may help predict how the coupled joints of a knee-ankle prosthesis would need to move to achieve reduced hip compensation. To demonstrate the potential utility of understanding healthy coordination, we provide an example in Fig. 10, where the shank profile that would be necessary to achieve AB coordination and desired healthy thigh behavior given a passive prosthetic foot trajectory is predicted. Specifically, in this example we imposed the mean CVP of AB gait as a *constraint* for the TFA to theoretically follow. Since our goal would be to achieve healthy thigh angle/moment for a TFA prescribed with a passive prosthetic foot, we aim to identify the necessary shank angle/moment that would coordinate with the thigh and foot segments based on the healthy AB constraint. Based on this shank angle/moment and the transformation approach previously described, a controller could be designed to coordinate ankle and knee joints to achieve a desired hip profile.

We evaluated our reduced Jacobian method (J_α) by comparing the reconstructed powers in section III-D. The powers for AB subjects were reconstructed by the 3-DOF ESM with a relative RMSE of $6.5\% \pm 2.2\%$. This difference likely arises from the reduced Jacobian assumption, which may in part also explain the lower PI in the amputated legs of TFA subjects compared to AB subjects in ESM (see Figure 6). This provides motivation to expand our Jacobian to a full-order Jacobian ($J \in \mathbb{R}^{12 \times 12}$), and extend ISC to 3D, both in elevation angles and in elevation space moments.

Expanding on this work we aim to better understand the role of coordination in 3D dynamics of gait, in simulation and experiments, to further elucidate the relationship between coordination and energetics. Previously, the results from [9] showed a strong correlation between mechanical energy cost and the CVP. While the causality of this correlation is as yet indeterminate, we believe that extending ISC from kinematics to dynamic coordination could help address this fundamental question. Ultimately, the goal is to develop a means to reduce metabolic cost based on a deeper under-

standing of dynamic coordination and its ties to energetics.

Though reporting joint angles has become standard for the evaluation of human movement, angles/moments in elevation coordinates have been shown here to reveal attributes of human motion that are not evident when considering angles/moments in joint coordinates alone. This provides motivation to the biomechanics community to report empirical gait data in elevation coordinates when possible. Our ISC3d toolbox was developed explicitly with the goal to facilitate the use of elevation angles for such comparisons. Critically, the broader question of whether the human nervous system is controlled in joint or global coordinates is one that remains an open question within the field of study of neural control of movement [31], [32].

Moreover, the origin of ISC is an open question. Inter-segmental coordination may represent a objective function of the Central Nervous System (CNS) for reducing the dimensionality of gait, and it remains an open area of debate whether the coordination is a controlled variable in human motor control [11], [33], or merely a kinematic result of a mechanical performance metric [34].

Importantly, in this work, we introduced a method (see section II-C) to compute elevation angles from 3D anatomical joint angles to make intersegmental coordination analysis more accessible. We extended this approach into a novel method (see section II-D) to compute moments in elevation angle space, defined as the elevation space moments (ESM), which is freely available in our ISC3d toolbox [30]. In traditional methods, the elevation angles are computed solely based on marker data, avoiding the need for calculating a transformation between anatomical joint angles to elevation angles. However, without this transformation it is impossible to then transform other variables, such as joint moments, to the same subspace where coordination is achieved. This is why the extension of ISC from kinematics to dynamics has not been performed previously, to our knowledge.

APPENDIX

A. Sign Conventions and Definitions

Equations (2) to (5) require sign corrections (see Table II) depending on laterality and anatomical angle definitions.

TABLE II: Sign corrections for joint rotations based on laterality.

Joint	Component	Left (L)	Right (R)
Pelvis	Tilt	$R_z(-\phi_p)$	$R_z(-\phi_p)$
	Obliquity	$R_x(+\delta_p)$	$R_x(-\delta_p)$
	Rotation	$R_y(+\rho_p)$	$R_y(+\rho_p)$
Hip	Flexion	$R_z(+\phi_h)$	$R_z(+\phi_h)$
	Adduction	$R_x(-\delta_h)$	$R_x(+\delta_h)$
	Rotation	$R_y(-\rho_h)$	$R_y(+\rho_h)$
Knee	Flexion	$R_z(-\phi_k)$	$R_z(-\phi_k)$
	Adduction/Varus	$R_x(-\delta_k)$	$R_x(+\delta_k)$
	Rotation	$R_y(-\rho_k)$	$R_y(+\rho_k)$
Ankle	Dorsiflexion	$R_z(\phi_a + 90^\circ)$	$R_z(\phi_a + 90^\circ)$
	Rotation	$R_x(-\rho_a)$	$R_x(+\rho_a)$
	Inversion	$R_y(+\delta_a)$	$R_y(-\delta_a)$

This is further explained in our ISC3d toolbox [30]. Joint angles follow Vicon Plug-In Gait definitions of anatomical angles [35]. Reference frames for transformations follow ISB recommendation [27]. For the j^{th} joint, we denote anatomical angles as flexion (ϕ_j), adduction (δ_j) and rotation (ρ_j). The joint angles vector (q) in (13), is defined in (17).

$$q = [\phi_p, \delta_p, \rho_p, \phi_h, \delta_h, \rho_h, \phi_k, \delta_k, \rho_k, \phi_a, \delta_a, \rho_a] \quad (17)$$

The joint torque vector (τ) used in (12), is defined in (18). It contains hip (τ_h), knee (τ_k), and ankle (τ_a) torques in three axes $\tau_j = [\tau_{\phi_j}, \tau_{\delta_j}, \tau_{\rho_j}]$, augmented with zeros to match the dimensions of $q \in \mathbb{R}^{12}$ and J_α .

$$\tau = [0_{1 \times 3}, \tau_h, \tau_k, \tau_a]^T \quad (18)$$

REFERENCES

- [1] L. Van Schaik, J. H. B. Geertzen, P. U. Dijkstra, and R. Dekker, “Metabolic costs of activities of daily living in persons with a lower limb amputation: A systematic review and meta-analysis,” *PLOS ONE*, vol. 14, no. 3, p. e0213256, Mar. 2019.
- [2] R. Gailey, K. Allen, J. Castles, J. Kucharik, and M. Roeder, “Review of secondary physical conditions associated with lower-limb amputation and long-term prosthesis use,” *Journal of Rehabilitation Research and Development*, vol. 45, no. 1, pp. 15–29, 2008.
- [3] D. A. Winter, *Biomechanics and motor control of human gait: normal, elderly and pathological*, 2nd ed. University of Waterloo Press, 1991.
- [4] F. Sup, A. Bohara, and M. Goldfarb, “Design and Control of a Powered Transfemoral Prosthesis,” *The International Journal of Robotics Research*, vol. 27, no. 2, pp. 263–273, Feb. 2008.
- [5] M. Tran, L. Gabert, S. Hood, and T. Lenzi, “A lightweight robotic leg prosthesis replicating the biomechanics of the knee, ankle, and toe joint,” *Science Robotics*, vol. 7, no. 72, p. eab03996, 2022.
- [6] S. K. Au, J. Weber, and H. Herr, “Powered Ankle–Foot Prosthesis Improves Walking Metabolic Economy,” *IEEE Transactions on Robotics*, vol. 25, no. 1, pp. 51–66, Feb. 2009.
- [7] N. Hogan, “Impedance Control: An Approach to Manipulation: Part II—Implementation,” *Journal of Dynamic Systems, Measurement, and Control*, vol. 107, no. 1, pp. 8–16, Mar. 1985.
- [8] R. Gehlhar, M. Tucker, A. J. Young, and A. D. Ames, “A review of current state-of-the-art control methods for lower-limb powered prostheses,” *Annual Reviews in Control*, vol. 55, pp. 142–164, 2023.
- [9] L. Bianchi, D. F. Angelini, G. P. Orani, and F. Lacquaniti, “Kinematic coordination in human gait: relation to mechanical energy cost,” *Journal of Neurophysiology*, vol. 79, no. 4, pp. 2155–2170, Apr. 1998.
- [10] N. A. Borghese, L. Bianchi, and F. Lacquaniti, “Kinematic determinants of human locomotion,” *The Journal of Physiology*, vol. 494, no. 3, pp. 863–879, Aug. 1996.
- [11] Y. P. Ivanenko, G. Cappellini, N. Dominici, R. E. Poppele, and F. Lacquaniti, “Modular Control of Limb Movements during Human Locomotion,” *Journal of Neuroscience*, vol. 27, no. 41, pp. 11149–11161, Oct. 2007.
- [12] Y. P. Ivanenko, A. d’Avella, R. E. Poppele, and F. Lacquaniti, “On the Origin of Planar Covariation of Elevation Angles During Human Locomotion,” *Journal of Neurophysiology*, vol. 99, no. 4, pp. 1890–1898, Apr. 2008.
- [13] A. H. Dewolf, Y. P. Ivanenko, K. E. Zelik, F. Lacquaniti, and P. A. Willems, “Kinematic patterns while walking on a slope at different speeds,” *Journal of Applied Physiology*, vol. 125, no. 2, pp. 642–653, Aug. 2018.
- [14] S. D. Israeli-Korn, A. Barliya, C. Paquette, E. Franzén, R. Inzelberg, F. B. Horak, and T. Flash, “Intersegmental coordination patterns are differently affected in Parkinson’s disease and cerebellar ataxia,” *Journal of Neurophysiology*, vol. 121, no. 2, pp. 672–689, 2019.
- [15] N. Krausz and T. Flash, “Asymmetric Changes in Intersegmental Covariation Across Ambulation Levels and Prosthetic Devices for Transfemoral Amputee Gait,” in *2023 11th International IEEE/EMBS Conference on Neural Engineering (NER)*, Apr. 2023, pp. 1–6.
- [16] E. R. Westervelt, J. W. Grizzle, C. Chevallereau, J. H. Choi, and B. Morris, *Feedback Control of Dynamic Bipedal Robot Locomotion*, 1st ed. CRC Press, Oct. 2018.
- [17] R. D. Gregg, T. Lenzi, L. J. Hargrove, and J. W. Sensinger, “Virtual Constraint Control of a Powered Prosthetic Leg: From Simulation to Experiments With Transfemoral Amputees,” *IEEE Transactions on Robotics*, vol. 30, no. 6, pp. 1455–1471, Dec. 2014.
- [18] T. K. Best, K. R. Embry, E. J. Rouse, and R. D. Gregg, “Phase-variable control of a powered knee–ankle prosthesis over continuously varying speeds and inclines,” in *2021 IEEE/RSJ International Conference on Intelligent Robots and Systems (IROS)*, 2021, pp. 6182–6189.
- [19] T. K. Best, C. G. Welker, E. J. Rouse, and R. D. Gregg, “Data-Driven Variable Impedance Control of a Powered Knee–Ankle Prosthesis for Adaptive Speed and Incline Walking,” *IEEE Transactions on Robotics*, vol. 39, no. 3, pp. 2151–2169, Jun. 2023.
- [20] R. J. Cortino, T. K. Best, and R. D. Gregg, “Data-Driven Phase-Based Control of a Powered Knee-Ankle Prosthesis for Variable-Incline Stair Ascent and Descent,” *IEEE Transactions on Medical Robotics and Bionics*, vol. 6, no. 1, pp. 175–188, Feb. 2024.
- [21] R. Gehlhar, J. Reher, and A. D. Ames, “Control of separable subsystems with application to prostheses,” 2022. [Online]. Available: <https://arxiv.org/abs/1909.03102>
- [22] L. M. Sullivan, M. Cowan, L. Gabert, and T. Lenzi, “Unified Control of a Powered Knee-Ankle Prosthesis Enables Walking, Stairs, Transitions, and Other Daily Ambulation Activities,” *IEEE Transactions on Neural Systems and Rehabilitation Engineering*, vol. 33, pp. 3024–3039, 2025.
- [23] D. A. Winter, “Overall principle of lower limb support during stance phase of gait,” *Journal of Biomechanics*, vol. 13, no. 11, pp. 923–927, Jan. 1980.
- [24] A. L. Hof, “On the interpretation of the support moment,” *Gait & Posture*, vol. 12, no. 3, pp. 196–199, Dec. 2000.
- [25] E. Reznick, K. R. Embry, R. Neuman, E. Bolívar-Nieto, N. P. Fey, and R. D. Gregg, “Lower-limb kinematics and kinetics during continuously varying human locomotion,” *Scientific Data*, vol. 8, no. 1, p. 282, Oct. 2021. [Online]. Available: <https://doi.org/10.1038/s41597-021-01057-9>
- [26] T. Elery, S. Rezazadeh, E. Reznick, L. Gray, and R. D. Gregg, “Effects of a Powered Knee-Ankle Prosthesis on Amputee Hip Compensations: A Case Series,” *IEEE Transactions on Neural Systems and Rehabilitation Engineering*, vol. 28, no. 12, pp. 2944–2954, Dec. 2020.
- [27] G. Wu and P. R. Cavanagh, “ISB recommendations for standardization in the reporting of kinematic data,” *Journal of Biomechanics*, vol. 28, no. 10, pp. 1257–1261, 1995.
- [28] R. M. Murray, Z. Li, and S. S. Sastry, *A Mathematical Introduction to Robotic Manipulation*, 1st ed. CRC Press, Dec. 2017.
- [29] B. Siciliano and O. Khatib, Eds., *Springer Handbook of Robotics*. Berlin, Heidelberg: Springer, 2008.
- [30] E. Siman Tov, “ISC3d,” Jan. 2026. [Online]. Available: <https://www.mathworks.com/matlabcentral/fileexchange/182726-isc3d>
- [31] R. Grasso, L. Bianchi, and F. Lacquaniti, “Motor patterns for human gait: Backward versus forward locomotion,” *Journal of Neurophysiology*, vol. 80, no. 4, pp. 1868–1885, Oct. 1998.
- [32] A. Barliya, N. Krausz, H. Naaman, E. Chiovetto, M. Giese, and T. Flash, “Human arm redundancy: a new approach for the inverse kinematics problem,” *Royal Society Open Science*, vol. 11, no. 2, p. 231036, Feb. 2024.
- [33] A. Barliya, L. Omlor, M. A. Giese, and T. Flash, “An analytical formulation of the law of intersegmental coordination during human locomotion,” *Experimental Brain Research*, vol. 193, no. 3, pp. 371–385, Mar. 2009.
- [34] H. Hicheur, A. V. Terekhov, and A. Berthoz, “Intersegmental Coordination During Human Locomotion: Does Planar Covariation of Elevation Angles Reflect Central Constraints?” *Journal of Neurophysiology*, vol. 96, no. 3, pp. 1406–1419, Sep. 2006.
- [35] *Plug-in Gait Reference Guide*, Vicon Motion Systems Ltd., Oxford, UK, 2023. [Online]. Available: <https://help.vicon.com/space/Nexus216/11607059/Plug-in+Gait+Reference+Guide>